ROYAL SOCIETY
OF CHEMISTRY

COMMUNICATION

Check for updates

Rheological responses of microgel suspensions with temperature-responsive capillary networks†

Zhecun Guan,[a] Lisa Tang[ab] and Jinhye Bae ✉*[abc]

A method coupling microgel jamming and temperature-responsive capillary networking is developed to manipulate the rheological properties of microgel-capillary suspensions by varying microgel sizes, volume fraction of capillary solution, and temperature after polymerization and photo-crosslinking. This approach allows for the 3D extrusion of this suspension to print complex structures that can be readily scaled up and applied to biomedical fields and soft material-based actuation.

Introduction

Hydrogels are water-swollen polymeric materials that exhibit softness, deformability, and high water content with structures akin to native tissue properties due to their hydrophilic polymer networks.[1–3] In general, hydrogels are crosslinked in bulk, which results in a mesh-like matrix with nanoscale porosity, but may limit the mass transport of water in response to the environmental changes because of their low interfacial areas.[4,5] Granular hydrogels have recently emerged as a promising platform to address the structural limitations of bulky hydrogels.[6] Granular hydrogels have a collection of hydrogel microparticles (*i.e.*, microgels) that generally have a diameter greater than 10 μm. Above this size the gravitational forces overwhelm the thermal fluctuations.[7] In addition, the van der Waals force between adjacent microgels is nominal relative to friction.[8] Therefore, these granular microgels can form a jammed state, in which the packed disordered microgels are immobilized by surrounding microgels through their physical interactions and transfer from a liquid-like state to solid-like paste when the

particle-to-volume ratio is higher than 0.58, which is defined as random loose packing.[9] The injectable characteristics of jammed microgels due to their shear thinning behaviors have recently been exploited in three-dimensional (3D) printing techniques.[10] Burdick and co-workers harnessed two kinds of hyaluronic acid microgels that are chemically modified with either hydrazide or aldehyde groups and mixed them while 3D printing to form microgel systems containing a dynamic hydrazone bond.[11] Similarly, Saunders and co-workers established the interlinking of two types of microgels through covalent bonds.[12] Burdick group further proved the diversity of microgel inks with various crosslinking mechanisms for 3D printing applications, including radical chain-growth polymerization, thiol-ene photoinitiated crosslinking, and thermally-induced physical crosslinking.[13] Furthermore, Huang and co-workers employed gelatin microgels as rheological modifiers in gelatin solution for cell-laden printing due to the effect of physical crosslinking and thermal gelation at room temperature.[14] However, these strategies generally require an interparticle connection by chemical bonding or physical crosslinking to stabilize the microgels, which impedes the versatility of microgel systems.

As a non-covalent interaction between microgels, capillary forces have been utilized to form microgel networks (*i.e.*, capillary suspensions) that can stabilize microgel suspensions and tune their rheological properties.[15,16] Specifically, the capillary solution wets the microgels more than the primary fluid that originally surrounded the microgels.[17] Therefore, microgels are linked to each other *via* capillary bridges to form clusters of microgels.[18] Furthermore, the interlinking of microgels by capillary solutions can lead to a transition from fluid-like to gel-like behavior and enhance the mechanical strengths.[19,20] Velev and co-workers employed an uncured liquid precursor to assemble polydimethylsiloxane (PDMS) microbeads in aqueous phase by capillary attraction.[21] The capillary suspensions possess high storage moduli and yield stresses that facilitate 3D printing. In addition, the stability of microgel suspensions is improved due to the formation of capillary networks, and thus

[a] Department of NanoEngineering, University of California San Diego, La Jolla, CA 92093, USA

[b] Chemical Engineering Program, University of California San Diego, La Jolla, CA 92093, USA

[c] Materials Science and Engineering Program, University of California San Diego, La Jolla, CA 92093, USA. E-mail: j3bae@ucsd.edu

prevents phase separation between water and oil, so that the microgel suspension can be stable for longer periods of time without the need to remix or agitate before use.[22] Recently, Mohraz and co-workers utilized capillary solutions for temperature-responsive bicontinuous interfacially jammed emulsion gels (*i.e.*, bijel) and studied the role of capillary solutions in bijel systems *via* rheological characterization.[23] However, to the best of our knowledge, temperature-responsive capillary networks have not been employed for microgel suspensions to realize temperature-responsive rheological properties.

Here, we couple jammed microgels and the temperature-responsive capillary network to develop a new strategy that not only substitutes the chemical modification and physical crosslinking with the capillary bridges between the microgels, but also exhibits temperature-responsive behavior after cross-linking the capillary solution. Polyacrylamide (PAAm) microgels are fabricated with a water-in-oil emulsion template using mechanical agitation, radical polymerization, and photo-crosslinking by UV irradiation. The crosslinkable poly(*N*-isopropylacrylamide) (PNIPAm) precursor solution serves as a capillary solution in this system to provide capillary networking as well as temperature responsiveness after photo-crosslinking due to the lower critical solution temperature (LCST) of PNIPAm ranging from 30 to 50 °C.[24] The rheological behaviors are manipulated by different microgel sizes and different volume fractions of PNIPAm precursor introduced into the microgel suspensions to allow for 3D extrusion printing without the addition of other rheological modifiers or surface modification of microgels. We further demonstrate the printability of microgel-capillary suspensions to build complex 2D and 3D structures. Due to the temperature-responsive capillary network, such printed structures exhibit temperature-responsive rheology and volume change after the polymerization and photo-crosslinking of capillary networks. The stimuli-responsive capillary networks will pave a new way to tune the rheological behaviors of the microgel-based systems by physical factors as well as external stimuli, thus they can be readily 3D printed into desired structures and dimensions for various applications including biomedical engineering, soft actuators, and wearable sensors.

Results

To date, multiple methods for fabricating microgels have been developed including microfluidic devices, batch emulsions, and mechanical fragmentation.[25–27] Burdick and co-workers systematically characterized the influence of microgel fabrication techniques of granular microgels on the resulting properties of mechanics, porosity, and injectability.[28] Despite the polydispersity of microgels, microfluidic and batch emulsification methods have similar values for their storage modulus and porosity. In this work, we select the batch emulsification method to prepare PAAm microgels *via* a water-in-oil emulsification because of its simplicity and high yield. The aqueous PAAm precursor is composed of acrylamide (AAm) as a monomer, *N*,*N*-methylenebisacrylamide (BIS) as a crosslinker and
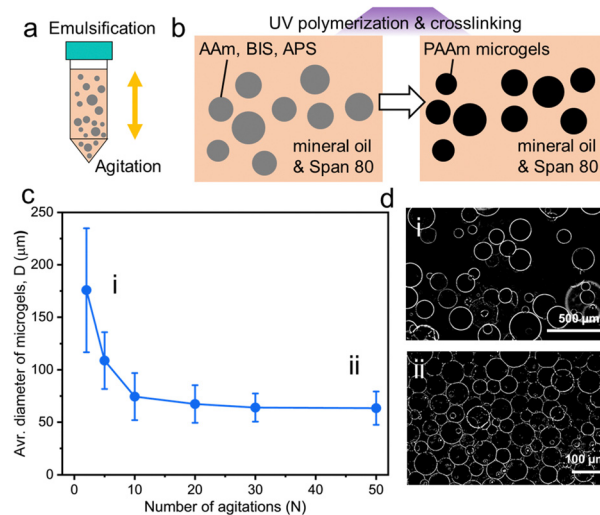

Fig. 1 Preparation and the size control of PAAm microgels. (a) Water-in-oil emulsification with different droplet sizes controlled by the number of agitations. (b) Polymerization and crosslinking of PAAm precursor droplets by UV irradiation. (c) The effect of the number of agitations (*N*) in average diameters of PAAm microgels (*D*). (d) Thresholded Z-slice optical microscope images of (i) large (*N* = 2) and (ii) small (*N* = 50) microgels, respectively.

ammonium persulfate (APS) as a photo-initiator. Mineral oil is used as the oil phase because it has a much lower O_2 solubility than other types of oil commonly used in emulsification methods, which ensures that radical polymerization reactions are not inhibited by the presence of oxygen.[29,30] Water-in-oil emulsions are prepared by agitating the mixture of aqueous PAAm microgel precursor solution and the oil phase containing Span 80 surfactants (Fig. 1a). Upon UV irradiation, PAAm precursor droplets (*i.e.*, the dispersed phase) are photo-polymerized and crosslinked to form PAAm microgels (Fig. 1b). These fabricated microgels are washed using mineral oil and the full removal of the redundant surfactants is confirmed by FTIR (Fig. S1, ESI†). Both C–H stretching and C–O stretching vibration of Span 80 with characteristic peaks at 2855 cm^{-1} and 1173 cm^{-1}, respectively, disappear after oil washing three times.[31] After oil washing, the PAAm microgels/mineral oil mixture is centrifuged to separate the upper oil layer and jammed microgel suspensions at the bottom of the centrifuge tube. DI water is added to each batch of the microgel suspensions to dilute them to 20:1 ratio and allow the microgels to fully swell for 24 hours before measuring the microgel sizes.

The number of agitations (*N*) in mixing aqueous and oil phases is used to control the sizes of both the PAAm precursor droplets and microgels after photo-crosslinking and polymerization. The size distribution of swelled microgels at their equilibrium state is characterized by optical microscopy and over 100 microgels for each *N* were measured. The manipulation of the size of PAAm precursor droplets results in diameters of microgels (*D*) ranging from 176 ± 59 μm (*N* = 2) to 63 ± 16 μm (*N* = 50) as shown in Fig. 1c. The average *D* dramatically decreases from 176 μm to 74 μm when *N* rises from 2 to 10, it then decreases to 64 μm when *N* reaches 30 and remains

similar (from 64 μm to 63 μm) when N increased from 30 to 50. Image thresholding is used to create binary images that clearly illustrate microgels from the backgrounds. Representative thresholded Z-slice optical microscope images of large microgels at $N = 2$ and small microgels at $N = 50$ are shown in Fig. 1d. The polydispersity of large microgels is higher than their small counterparts, which is further quantified by the coefficient of variation (CV). The CV of large microgels ($N = 2$) is 33.58%, while the results for relatively smaller microgels are 21.01% ($N = 30$) and 25.14% ($N = 50$) (Fig. S2, ESI†).

After fabricating PAAm microgels with different sizes, we characterized the effect of microgel size on the rheological properties of PAAm microgel suspensions. To determine the linear shear moduli including shear elastic modulus (G') and viscous modulus (G''), we performed the oscillatory frequency sweeps spanning frequencies of 0.001 Hz to 10 Hz at a low strain amplitude of 1% (Fig. 2a). Microgel suspensions exhibit increased G' and G'' with an increased average D. Notably, the suspension containing large microgels with a size range of 176 ± 59 μm shows a G' of 1651 Pa which is 4-fold higher than those with small microgels with 63 ± 16 μm diameters. To quantify the yield stress of each emulsion formulation, the shear stress with shear rates covering 100 s^{-1} to 0.001 s^{-1} is examined in Fig. 2b. The plateau ranges from 10 to 0.01 s^{-1} on a log scale, which corresponds to the linear viscoelastic region. The suspension containing PAAm microgels with an average size of 63 μm contribute to a viscosity of 52 Pa s, whereas larger microgels of 176 ± 59 μm exhibit a much greater viscosity of 120 Pa s at 1.0 s^{-1} (Fig. 2c).

In general, rheological properties of microgel suspensions depend on their shape,[32] size,[33] polydispersity,[28] stiffness,[34] and external conditions (*e.g.*, temperature and pressure[23,35]). In this work, a close packing of relatively larger microgels provides a large interparticle contact area because of a higher microgel size dispersity, which generates increased friction between microgels in microgel suspensions. On the other hand, smaller sizes and a lower size dispersity of PAAm microgels produce a loose packing in microgel suspensions. Therefore, microgel suspensions containing relatively larger microgels exhibit higher values in both G' and viscosity compared with their smaller counterparts.

Fig. 2 Rheological characterization of jammed PAAm microgel suspensions. (a) Small amplitude oscillatory frequency sweeps that determine G' (solid circles) and G'' (hollow circles). (b) Shear rate sweeps that determine the yield stress of PAAm microgel suspensions. (c) Viscosity@1.0 s^{-1} for PAAm microgels suspensions with different average D.

We investigated the size effect of microgels on the rheological behaviors of microgel suspensions, however, covalent bonding hugely limits the diversity of microgel platforms for various fields that requires scale-ups and complex 2D or 3D structures.[36] To overcome this issue, a crosslinkable PNIPAm precursor is employed as the capillary solution to introduce the additional interparticle interactions thus controlling the rheological responses of microgel suspensions. Using the same feed ratio of the monomer and the initiator (4 wt%) as we originally employed in the capillary solution except for the photo-crosslinker, the molecular weight (M_W) of the linear PNIPAm was measured 9.7×10^5 ($\pm$ 18.1%) g mol^{-1} (Fig. S3, ESI†).

Contact angle measurements are performed to compare the wettability of PAAm/mineral oil and PAAm/PNIPAm precursor. The contact angle of mineral oil on PAAm layer is $36.6 \pm 4.1°$, while this value for PNIPAm precursor is $24.7 \pm 1.5°$ (Fig. 3a). PNIPAm precursor shows a relatively greater wettability on the PAAm microgel surface compared to the mineral oil phase. Hence, the microgel-capillary networks can form upon the addition of the PNIPAm precursor and adequate mixing as illustrated in Fig. 3b. To visualize the capillary networks, rhodamine B (RhB) is conjugated to 2-hydroxyethyl methacrylate (HEMA) to produce rhodamine B-conjugated 2-hydroxyethyl methacrylate (RhB-HEMA) and thus fluorescently label PNIPAm precursors (Fig. S4, ESI†). The characteristic peak of unsaturated –C=C– at 4.83 ppm in ^{1}H-NMR spectroscopy of the fabricated RhB-HEMA confirms the conjugation of RhB to HEMA monomer. The subsequent photo-initiated copolymerization between RhB-HEMA and NIPAm at room temperature is described in Fig. 3c. The feed ratio of RhB-HEMA and NIPAm is remained at $1:20$ for all the fluorescent imaging. Fig. 3d presents a 3D confocal fluorescence microscopic image, which shows a high fluorescence intensity of capillary solution in the surroundings around each microgel and the interlinking between adjacent microgels.

The volume fraction of the capillary solution in microgel-capillary suspensions is defined as $\Phi_{PNIPAm} = V_{PNIPAm\ precursor}/V_{PAAm\ microgel\ suspension}$, where $V_{PNIPAm\ precursor}$ represents the volume of PNIPAm precursor solution and $V_{PAAm\ microgel\ suspension}$ indicates the volume of the PAAm microgel suspension. For a systematic study to understand the role of the capillary solution, we conduct rheological characterization on microgel-capillary suspensions as a function of Φ_{PNIPAm}. When Φ_{PNIPAm} is increased from 0.04 to 0.17, the "bridging" liquid further wets the surface of microgels, as shown in Fig. S5a and b (ESI†), respectively.

The different stress and viscosity behaviors of microgel-capillary suspensions compared to microgel suspensions can indicate the presence of capillary interactions between PAAm microgels (Fig. S6, ESI†). In general, G' measured at 100 Hz increases and then decreases with an increasing Φ_{PNIPAm} ranging from 0 to 0.08, as shown in Fig. 3e. Similarly, Fig. 3f records an up-and-down trend as the viscosity measured at 1.0 s^{-1} of microgel-capillary suspension varies with Φ_{PNIPAm}. For instance, G' of the microgel-capillary suspension with an average D of 63 μm summit when $\Phi_{PNIPAm} = 0.08$. We then compared the rheological responses for microgel-capillary

Fig. 3 Effect of the capillary solution in microgel–capillary suspensions. (a) Contact angle measurements of mineral oil and PNIPAm precursor droplets on PAAm layers, respectively. (b) Scheme of the formation of microgel–capillary networks. (c) Copolymerization of RhB-HEMA and NIPAm *via* photo-crosslinking. (d) 3D confocal fluorescence microscopic image exhibiting the location of capillary solution between microgels. The red fluorescent signal indicates the existence of RhB-HEMA in the PNIPAm precursor capillary solution. (e) G'@100 Hz as a function of Φ_{PNIPAm} in microgel–capillary suspensions. (f) Viscosity@1.0 s^{-1} as a function of Φ_{PNIPAm} in microgel–capillary suspensions.

suspensions with different microgel sizes. Remarkably, G' increases from 1980 to 2683 Pa and viscosity rises from 120 to 398 Pa s for microgel–capillary suspensions containing microgels of 176 ± 59 μm, while their counterparts containing smaller microgels of 63 ± 16 μm show an increase from 417 to 571 Pa in G' and 52 to 62 Pa s in viscosity. Furthermore, Φ_{PNIPAm} required to exhibit a maximum G' and viscosity slightly increases from 0.04 to 0.17 as the average D increases from 63 to 176 μm. This agrees with the claim that only a small fraction of capillary solution is required for microgel–capillary suspensions, otherwise the excess amount of the capillary solution may lead to agglomerates or Pickering emulsions.[37] It is demonstrated that the rheological responses of the microgel–capillary network depend on the microgel size and the volume fraction of capillary solution, owing to the presence of capillary interactions, area of contact, and polydispersity.[38] Besides, the increasing trend of G' and viscosity until maximum confirms that the capillary interaction is larger than the interparticle friction of microgels in a jammed state. As control groups, the frequency sweep and strain sweep of the capillary solution are performed (Fig. S7, ESI†). The shear moduli of the capillary solution ranges from 10^{-4} to 10^{2} Pa and the viscosity remains within 10^{-3} to 10^{-1} Pa s, which are negligible compared with the values of microgel suspensions. This confirms that the rheology of microgel–capillary networks is not a simple summation of the rheology of microgel suspensions and a capillary solution, but a result of capillary networks.

The 3D printability of the paste-like microgel–capillary suspensions are examined because of their shape retaining ($G' > G''$) and shear-thinning behaviors.[39] Fig. 4a illustrates the 3D extrusion printing of microgel–capillary suspensions and the bright-field and fluorescent micrographs of the microgel–capillary suspension ink. Jammed PAAm microgels are shown in the bright-field optical micrograph and the PNIPAm capillary networks between adjacent microgels are located with higher contrast in red color in the fluorescent micrograph. The microgel–capillary suspension ink (Φ_{PNIPAm} = 0.17, D = 109 ± 27 μm) is first printed into the 2D curved structures "UCSD" on a glass slide with a 20 mm s^{-1} printing speed under 30 kPa pneumatic pressure using a 22-gauge (0.41 mm inner diameter) dispensing needle (Fig. S8a and Video S1, ESI†). After that, the printed structures of the microgel–capillary suspensions are transferred to a homemade transparent humid box to prevent drying out during UV irradiation. The UV irradiation initiates the radical polymerization and crosslinking of NIPAm and immobilizes PAAm microgels. After immersing in DI water, the fully swelled crosslinked letters can freely float in water, which confirms that crosslinked PNIPAm capillary networks are capable of stabilizing the printed structures (Fig. S8b, ESI†). Additionally, more complex lattice (10 × 10 mm) designs with different infill densities are printed using the same microgel–capillary suspension inks to further test the structural stability. Printing paths of different infill densities preserve well after UV
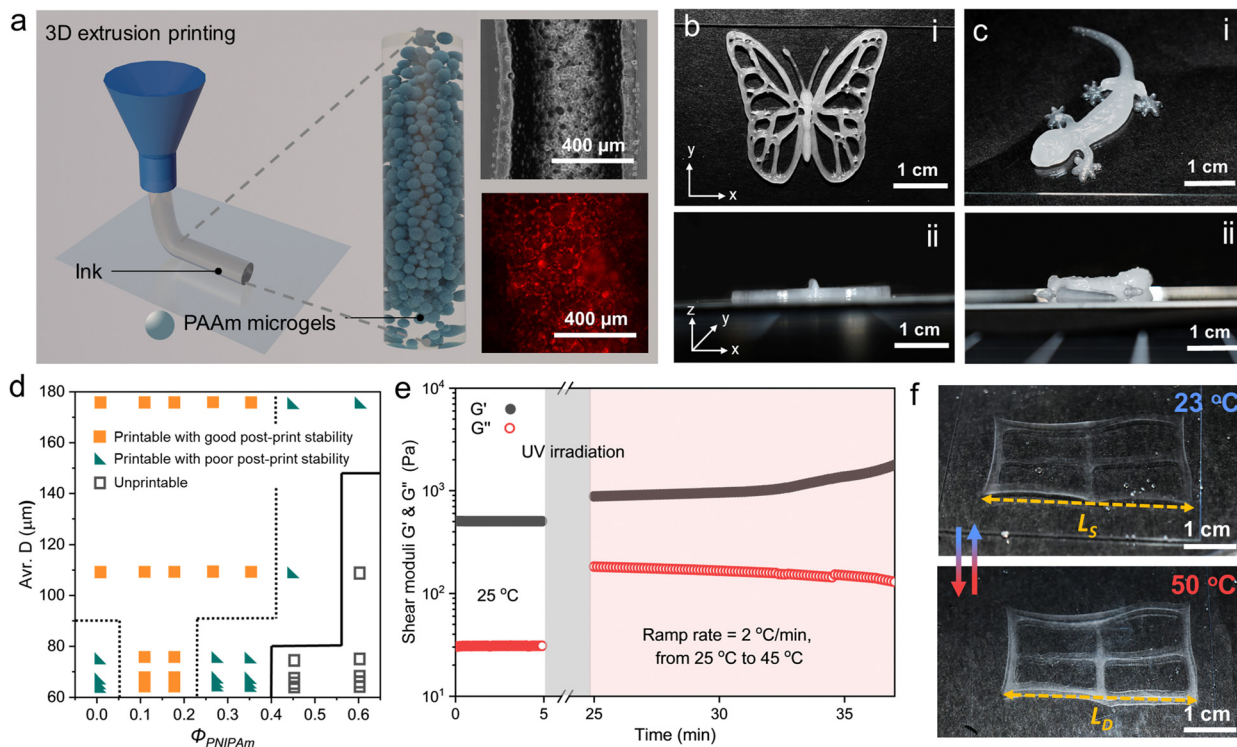
Fig. 4 3D extrusion printing of microgel-capillary suspension inks and the temperature responsiveness of the crosslinked printed structures. (a) Schematic of the 3D extrusion printing using microgel-capillary suspension inks and microscopic images of the ink in bright and fluorescent fields, respectively. (b and c) Top-view and side-view of the printed 3D butterfly and gecko structures. (d) The printability diagram of microgel-capillary network inks as a function of the average D and Φ_{PNIPAm}. The dashed lines indicate a boundary between printable inks with good or poor post-print stability, and the solid line distinguishes between the printable and unprintable inks. (e) Rheological responses of the microgel-capillary suspensions before and after crosslinking and polymerization as a function of the elevated temperature from 25 °C to 45 °C with a ramp rate of 2 °C min^{-1}. (f) The printed rectangular lattice structure in swelled and deswelled states in 23 °C and 50 °C water, respectively.

irradiation and swelling (Fig. S9, ESI†). For the better demonstration of the rheological enhancement for printing, we designed and printed intricate 3D butterfly and gecko structures, as shown in Fig. 4b and c, respectively. The clear printing paths of these structures confirm the excellent 3D printability and shape retention of our inks, especially through the Z-axis from the side views. Next, to examine the post-print stability of multi-layer stacking, we designed an 8-layer 3D cylinder lattice with a 5 mm radius, a 3 mm height, and a 15% infill density. Good post-print stability is confirmed when the printed 3D lattice can retain its shape longer than 30 min. On the other hand, if the lattice collapses within 30 min after printing, the ink will be classified as printable with poor post-print stability (Fig. S10 and Videos S2, S3, ESI†). In Fig. 4d, the printability diagram summarizes the printability of microgel-capillary suspensions as a function of the average D and Φ_{PNIPAm}. The inks are categorized as printable with good post-print stability, printable with poor post-print stability, and unprintable types. When the capillary solution is introduced to the microgel suspensions, the post-print stability is enhanced. However, the post-print stability of microgel-capillary ink starts to decrease when Φ_{PNIPAm} reaches 0.26. When Φ_{PNIPAm} is over 0.44, the inks will gradually lose their printability. PNIPAm capillary networks can retain the shapes after printing with

increased rheological properties and allow for free motion of the structures after polymerization and crosslinking.

To examine the temperature-dependent rheological responses of microgel-capillary suspensions, we conduct the oscillatory temperature evolution of G' and G'' following the formation of PNIPAm capillary networks from 25 to 45 °C with a ramp rate of 2 °C min^{-1} (Fig. 4e). With a UV intensity of 100 mW cm^{-2} for 20 min, microgel-capillary suspensions undergo polymerization and crosslinking, thus G' increases from 503 to 879 Pa and G'' rises from 31 to 183 Pa then remains stable until the temperature reaches 35 °C. The crosslinked PNIPAm capillary network presents temperature responsiveness in G' and G'' with an elevated temperature. We hypothesize that the PNIPAm capillary network perform a coil-to-globule transition when first heated up to LCST, then both PAAm microgels and PNIPAm capillary network lose water inside and shrink as the temperature increases to 45 °C.[40,41] To explore the temperature responsiveness of the printed structures, microgel-capillary suspension inks with different Φ_{PNIPAm} are polymerized and photo-crosslinked by UV irradiation. We use the microgel-capillary suspension ink with a Φ_{PNIPAm} of 0.17 to print a rectangular lattice with an infill density of 5%. The printed structure is swelled in water at 23 °C for 24 hours and then deswelled in 50 °C water for 5 hours. Linear swelling and deswelling ratios are employed to quantify the swelling and

Table 1 Swelling and deswelling ratios of the PAAm, PNIPAm and PAAm microgel/PNIPAm layers

Composition	Linear swelling ratio, λ_S	Linear deswelling ratio, λ_D
PNIPAm layer	1.109 ± 0.028	0.502 ± 0.019
PAAm layer	1.426 ± 0.139	1.423 ± 0.078
PAAm microgel-PNIPAm capillary network ($\Phi = 0.17$)	1.409 ± 0.017	1.237 ± 0.025
PAAm microgel-PNIPAm capillary network ($\Phi = 0.26$)	1.383 ± 0.020	1.178 ± 0.010
PAAm microgel-PNIPAm capillary network ($\Phi = 0.35$)	1.201 ± 0.026	0.936 ± 0.007
PAAm microgel-PNIPAm capillary network ($\Phi = 0.87$)	1.124 ± 0.016	0.811 ± 0.015

deswelling behaviors of the printed PAAm microgel/PNIPAm lattice. Linear swelling ratio (λ_S) is defined as $\lambda_S = L_S/L_0$, and linear deswelling ratio (λ_D) is defined as $\lambda_D = L_D/L_0$. L_0 is the equilibrium length of as-prepared layer at 23 °C, while L_S and L_D represent the equilibrium dimension of the layer at 23 °C and 50 °C, respectively. Upon heating to 50 °C, this printed structure turns translucent due to the LCST behavior of PNIPAm and shows a size shrinkage due to the deswelling of PNIPAm capillary networks with a λ_D of 1.24 (Fig. 4f). However, the 3D extrusion printing can lead to anisotropic swelling and deswelling because of the shear forces applied to the ink when extruded from a nozzle.[42]

Typically, hydrogels exhibit isotropic swelling when they are not physically constrained (*e.g.*, by substrates or shear forces), therefore, the linear swelling and deswelling ratios measured in thin films can determine the volumetric swelling and deswelling ratios and are similar to the ones measured from bulky structures.[43,44] To systematically study swelling and deswelling behaviors of microgel-capillary suspensions, we cast PNIPAm, PAAm, and PAAm microgel/PNIPAm into thin layers and summarize linear swelling and deswelling ratios in Table 1. The PAAm layers clearly show no deswelling behaviors thus no temperature responsiveness by changing temperature. The PNIPAm layers exhibit significant size changes, $\lambda_S = 1.109 \pm 0.028$ and $\lambda_D = 0.502 \pm 0.019$, upon cooling (23 °C) and heating (50 °C). For PAAm microgel/PNIPAm layers, both λ_S and λ_D vary between the ratios of PAAm and PNIPAm layers. It is demonstrated that microgel-capillary networks present decreasing λ_S and λ_D with a higher Φ_{PNIPAm}. In this manner, the swelling and deswelling behaviors of microgel-capillary networks can be controlled by changing Φ_{PNIPAm}.

In conclusion, we have developed a strategy to manipulate rheological responses of microgel suspensions that can further be used as ink materials for 3D extrusion printing. A cross-linkable PNIPAm precursor is applied to jammed PAAm microgel suspensions as a capillary solution that not only creates capillary interactions between PAAm microgels but also allows for stabilization of printed structures upon UV irradiation. Microgel suspensions of different PAAm microgel sizes have been fabricated *via* a water-in-oil emulsion methodology with different number of agitations. We have demonstrated that the rheological responses of microgel-capillary solutions can be controlled by microgel sizes and the volume fraction of the capillary solution. After polymerization and crosslinking, microgel-capillary networks perform temperature responsiveness and tunable swelling and deswelling behaviors with different volume fractions of PNIPAm capillary networks. We anticipate that our study will provide an in-depth understanding of the rheological responses of microgel-capillary networks and pave the way for the printing of 1D to 3D complex microgel structures. In the future, microgel-capillary network systems can be conveniently combined with other biological cells and other functional materials and show prospects in applications of flexible devices, soft actuators, and biomedical fields.

Author contributions

J. B. and Z. G. designed the project, analyzed the data and wrote the manuscript. Z. G conducted all the experiments. L. T. performed all fluorescent imaging.

Conflicts of interest

There are no conflicts to declare.

Acknowledgements

Notes and references

1 S. Van Vlierberghe, P. Dubruel and E. Schacht, *Biomacromolecules*, 2011, **12**, 1387–1408.
2 X. Liu, J. Liu, S. Lin and X. Zhao, *Mater. Today*, 2020, **36**, 102–124.
3 J. Kopeček, *Biomaterials*, 2007, **28**, 5185–5192.
4 C. Fan and D.-A. Wang, *Tissue Eng., Part B*, 2017, **23**, 451–461.
5 N. Annabi, J. W. Nichol, X. Zhong, C. Ji, S. Koshy, A. Khademhosseini and F. Dehghani, *Tissue Eng., Part B*, 2010, **16**, 371–383.
6 A. C. Daly, L. Riley, T. Segura and J. A. Burdick, *Nat. Rev. Mater.*, 2020, **5**, 20–43.
7 L. Riley, L. Schirmer and T. Segura, *Curr. Opin. Biotechnol*, 2019, **60**, 1–8.
8 K. Song, D. Zhang, J. Yin and Y. Huang, *Addit. Manuf.*, 2021, **41**, 101963.
9 E. R. Weeks, *Stat. Phys. Complex Fluids*, 2007, **2**, 87.

10 Q. Feng, D. Li, Q. Li, X. Cao and H. Dong, *Bioact. Mater.*, 2022, **9**, 105–119.

11 L. L. Wang, C. B. Highley, Y. C. Yeh, J. H. Galarraga, S. Uman and J. A. Burdick, *J. Biomed. Mater. Res., Part A*, 2018, **106**, 865–875.

12 A. H. Milani, J. Bramhill, A. J. Freemont and B. R. Saunders, *Soft Matter*, 2015, **11**, 2586–2595.

13 C. B. Highley, K. H. Song, A. C. Daly and J. A. Burdick, *Adv. Sci.*, 2019, **6**, 1801076.

14 K. Song, A. M. Compaan, W. Chai and Y. Huang, *ACS Appl. Mater. Interfaces*, 2020, **12**, 22453–22466.

15 K. Hauf and E. Koos, *MRS Commun.*, 2018, **8**, 332–342.

16 O. Fysun, S. Nöbel, A. J. Loewen and J. Hinrichs, *LWT*, 2018, **93**, 51–57.

17 S. Bindgen, J. Allard and E. Koos, *Curr. Opin. Colloid Interface Sci.*, 2021, 101557.

18 A. Ahuja and C. Gamonpilas, *Rheol. Acta*, 2017, **56**, 801–810.

19 Y. Fang, Y. Guo, M. Ji, B. Li, Y. Guo, J. Zhu, T. Zhang and Z. Xiong, *Adv. Funct. Mater.*, 2022, **32**, 2109810.

20 E. Koos, J. Johannsmeier, L. Schwebler and N. Willenbacher, *Soft Matter*, 2012, **8**, 6620–6628.

21 S. Roh, D. P. Parekh, B. Bharti, S. D. Stoyanov and O. D. Velev, *Adv. Mater.*, 2017, **29**, 1701554.

22 E. Koos, *Curr. Opin. Colloid Interface Sci.*, 2014, **19**, 575–584.

23 H. Ching and A. Mohraz, *Soft Matter*, 2022, **18**, 4227–4238.

24 S. Fujishige, K. Kubota and I. Ando, *J. Phys. Chem.*, 1989, **93**, 3311–3313.

25 S. Seiffert and D. A. Weitz, *Polymer*, 2010, **51**, 5883–5889.

26 Z. Li and T. Ngai, *Nanoscale*, 2013, **5**, 1399–1410.

27 D. Moon, M. G. Lee, J. Y. Sun, K. H. Song and J. Doh, *Macromol. Rapid Commun.*, 2022, **43**, 2200271.

28 V. G. Muir, T. H. Qazi, J. Shan, J. Groll and J. A. Burdick, *ACS Biomater. Sci. Eng.*, 2021, **7**, 4269–4281.

29 K. Sklodowska and S. Jakiela, *RSC Adv.*, 2017, **7**, 40990–40995.

30 J. Mandal, K. Zhang and N. D. Spencer, *Soft Matter*, 2021, **17**, 6394–6403.

31 X. Fu, W. Kong, Y. Zhang, L. Jiang, J. Wang and J. Lei, *RSC Adv.*, 2015, **5**, 68881–68889.

32 T. H. Qazi, J. Wu, V. G. Muir, S. Weintraub, S. E. Gullbrand, D. Lee, D. Issadore and J. A. Burdick, *Adv. Mater.*, 2022, **34**, 2109194.

33 M. Kessler, Q. Nassisi and E. Amstad, *Macromol. Rapid Commun.*, 2022, **43**, e2200196.

34 S. Franco, E. Buratti, B. Ruzicka, V. Nigro, N. Zoratto, P. Matricardi, E. Zaccarelli and R. Angelini, *J. Phys.: Condens. Matter*, 2021, **33**, 174004.

35 S. Adams, W. Frith and J. Stokes, *J. Rheol.*, 2004, **48**, 1195–1213.

36 T. H. Qazi, V. G. Muir and J. A. Burdick, *ACS Biomater. Sci. Eng.*, 2022, **8**, 1427–1442.

37 J. Guzowski, M. Tasinkevych and S. Dietrich, *Phys. Rev. E: Stat., Nonlinear, Soft Matter Phys.*, 2011, **84**, 031401.

38 F. Bossler and E. Koos, *Langmuir*, 2016, **32**, 1489–1501.

39 M. Shin, K. H. Song, J. C. Burrell, D. K. Cullen and J. A. Burdick, *Adv. Sci.*, 2019, **6**, 1901229.

40 L. Tang, L. Wang, X. Yang, Y. Feng, Y. Li and W. Feng, *Prog. Mater. Sci.*, 2021, **115**, 100702.

41 E. S. Gil and S. M. Hudson, *Biomacromolecules*, 2007, **8**, 258–264.

42 A. Sydney Gladman, E. A. Matsumoto, R. G. Nuzzo, L. Mahadevan and J. A. Lewis, *Nature materials*, 2016, **15**, 413–418.

43 E. M. White, J. Yatvin, J. B. Grubbs III, J. A. Bilbrey and J. Locklin, *J. Polym. Sci., Part B: Polym. Phys.*, 2013, **51**, 1084–1099.

44 N. Bouklas and R. Huang, *Soft Matter*, 2012, **8**, 8194–8203.